Multiresponse parameter estimation and compartmental analysis of time resolved fluorescence spectra. Application to conformational dynamics of charge-separated species in solution

van Stokkum, I.H.M.; Brouwer, A.M.; van Ramesdonk, H.J.; Scherer, T.

Publication date
1993

Published in
Proc.Kon.Ned.Akad.v.Wetensch.

Proc. Kon. Ned. Akad. v. Wetensch. 96 (1), 43–68 March 29, 1993

Multiresponse parameter estimation and compartmental analysis of time resolved fluorescence spectra

Application to conformational dynamics of charge-separated species in solution

I.H.M. van Stokkum[1], A.M. Brouwer[2], H.J. van Ramesdonk[2] and T. Scherer[2]

[1] *Faculty of Physics and Astronomy, Free University, De Boelelaan 1081, 1081 HV Amsterdam, the Netherlands*

[2] *Laboratory of Organic Chemistry, University of Amsterdam, Nieuwe Achtergracht 129, 1018 WS Amsterdam, the Netherlands*

Communicated by Prof. J.W. Verhoeven at the meeting of September 21, 1992

SUMMARY

Conformational changes of intramolecular charge-transfer species were studied by means of time resolved fluorescence spectroscopy. From a time resolved fluorescence spectrum the parameters which describe a kinetic, compartmental, model as well as the, model dependent, fluorescence spectral-shape parameters were estimated. We compared two methods for parameter estimation: nonlinear least squares and multiresponse. Analysis of residuals revealed shortcomings of the experimental set-up, in particular time jitter. The concentration fluctuations induced by this time jitter could cause failure of the usual nonlinear least squares model fit, whereas the multiresponse parameter estimation was successful.

Different compartmental models with the same kinetic parameters result in identical residuals. Thus a distinction can only be made on the basis of the accompanying estimated spectra. Due to the restriction that fluorescence spectra are nonnegative, the analysis of the two-component system 1 and system 2 (*scheme 1*) was only satisfactory using a model in which a slower decaying component was a reaction product of a faster decaying component. The three-component system 3 was satisfactorily described by a model with three independently decaying components.

INTRODUCTION

Time-resolved spectroscopy is widely used in chemistry, physics and biology to probe the kinetics of mixtures of components on a variety of timescales. In the fields of molecular photophysics and photochemistry electronic emission and transient absorption spectroscopy following an appropriately short pulse of radiation have proven their value over more than four decades now (Norrish and Porter 1948; Porter 1950). The problem of apparently complex kinetics due to the contribution of different species at a single wavelength can be addressed by

analysing time profiles measured at different wavelengths, as is often done in fluorescence studies using Single Photon Timing (Andriessen et al. 1991; Beechem et al. 1985; Cundall and Dale 1983; Löfroth 1985; Gust et al. 1991) or in nanosecond transient absorption spectroscopy (Nagle 1991; Solar et al. 1984; Visscher et al. 1988). Alternatively, for a wavelength range of interest spectra can be acquired at different time instants, an approach usually adopted in picosecond transient absorption spectroscopy and in the subpicosecond time domain.

The multiresponse (MR) parameter estimation method assumes that independent and identically distributed observations are made at several time instants of multiple responses measured at different wavelengths. The noise present with the responses may possess unknown, inconstant variance and may be correlated. In contrast, the usual nonlinear least squares (NLLS) parameter estimation method requires that the noise variance is constant, and that the responses are independent. In this article we apply both the MR and the NLLS analysis techniques to different sets of nanosecond time-resolved fluorescence data obtained using a time-gated optical multichannel analyser (OMA).

By means of time resolved spectroscopy the kinetics of a mixture of components whose spectra overlap can be measured indirectly by observing the total spectrum at several time instants. The perfect, noise-free, time resolved spectrum ψ is a superposition of the contributions of the n_{comp} different components:

$$\psi(t, \lambda) = \sum_{l=1}^{n_{comp}} c_l(t)\, \varepsilon_l(\lambda) \qquad \text{Eq. 1}$$

where $c_l(t)$ and $\varepsilon_l(\lambda)$ denote, respectively, the concentration and spectrum of component l.

Measurement of ψ poses the inverse problem: how can the spectroscopic and kinetic properties of the components be recovered. We will determine the number of components from the data and estimate the kinetic parameters using a compartmental model. Models with differential equations that are linear in the concentrations (like first order chemical reactions) are termed compartmental models (Anderson 1983; Godfrey 1983). A complication is that different compartmental models with the same kinetic parameters result in identical residuals.

These models differ only in their accompanying spectral parameters. Thus a priori knowledge about the spectra is necessary to choose between different candidate models. In the present paper we used the fact that the fluorescence intensity cannot be negative, but one could also make use of spectral shapes which are a priori supposed or independently measured on appropriate reference compounds.

We have recently studied several cases where the dynamics of fluorescence could be employed to monitor conformational changes of intramolecular charge-transfer species (Brouwer et al. 1991a,b; Scherer et al. 1991; Wegewijs et al. 1987, 1990). The molecules investigated consist of a photoexcitable cyanonaphthalene electron acceptor, an aromatic or aliphatic amine electron donor, and a semiflexible ring system linking the two. A characteristic feature is that even in nonpolar alkane solvents fast long-range electron transfer is possible in the ex-

tended ground state conformation in which the molecule exists immediately after excitation of the acceptor chromophore. Thus, a highly polar species is created, which can decrease its electrostatic energy by a conformational change in which donor and acceptor are brought close together. The exciplex-like species formed in this way emits fluorescence at a longer wavelength than the extended conformer. This folding process could be observed by means of time-resolved fluorescence spectroscopy. In addition, time-resolved microwave conductivity measurements were made which confirmed the change in dipole moment of the charge-separated species.

In this paper we present results obtained with the novel two-component systems **1** and **2**, and with the three-component system **3** (Brouwer et al. 1991a,b). The cases of compounds **1** and **2**, which feature two overlapping emission bands, illustrate clearly how the method of data analysis is used in conjunction with the physical requirement that the fluorescence intensity cannot be negative, in order to distinguish between three candidate kinetic models. In the case of **3** the analysis involves three components and is considerably more complicated, offering a choice between sixteen candidate kinetic models.

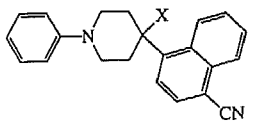

1 X = H
2 X = CN

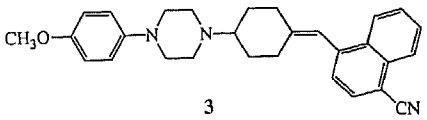

3

It is shown that the multiresponse analysis works in cases where the usual nonlinear least squares analysis is not appropriate because of inconstant variance of the residuals. The results of parameter estimation consist of a kinetic model with estimated rate constants as well as the (shapes of the) fluorescence emission spectra of the components. The examples demonstrate the power of our analytical methods, and at the same time reveal the practical limits imposed by the time resolution of our experimental setup.

METHODS

Experimental

The preparation of compounds **1**, **2** and **3** will be described elsewhere. For compounds **1** and **2** n-hexane was used as the solvent, compound **3** was studied in trans-decalin. Solvents used were commercial spectroscopic grade n-hexane (Merck Uvasol) and trans-decalin (Merck or Fluka) which was purified by the usual procedure for alkanes (Perrin et al. 1980). Solutions had an absorbance of about 0.1 in 1 cm at 308 nm and were deoxygenated by purging with argon for

at least 15 minutes. For excitation of the samples at 308 nm a Labda-Physik EMG 101 Xe/HCl excimer laser was used which produces pulses with an essentially Gaussian time profile with a width of about 7 ns and a power of 5–10 mJ/pulse. The laser was operated at a rate of 2–5 Hz. Fluorescence was detected at a right angle (through a cut-off filter in some cases) and collected by an optical fibre which led to a Jarrell-Ash monospec 27 model 1234 spectrograph in which the light was dispersed by a grating (150 grooves/mm) onto an MCP intensified diode array detector (EG&G 1421G, 25 mm, 1024 diodes). With this set-up a spectral range of about 600 nm was covered with a bandwidth of 5 nm (25 μm entrance slit) or 7 nm (250 μm slit). The detector was gated with a width of 5 ns by an EG&G 1302 pulse generator. The timing of the laser and Optical Multichannel Analyser (OMA) gate pulse was controlled by the EG&G OMA III model 1460 console with a 1303 pulse delay generator and a digital delay generator (EG&G model 9650).

Each experiment involved recording spectra at 15–45 different time instants with a constant time increment, or with a gradually increasing increment. At each time point spectra from 4–10 shots were averaged. In order to allow the experiment to be extended over a sufficiently large number of laser shots, without degradation of the sample, the laser pulse power was attenuated to less than 1 mJ/pulse by means of neutral density filters. This was necessary in particular in the case of compound **3**. The spectral intensities were not corrected for the wavelength dependent response of the detection system.

Steady state fluorescence spectra were recorded on a Spex Fluorolog II emission spectrometer, using an excitation wavelength of 300 nm.

Theoretical

The basic model which describes the time evolution of spectra is the following[1]:

$$\underline{\Psi}_{t_i\lambda_j} = \sum_{l=1}^{n_{\text{comp}}} c_{lt_i}\, \varepsilon_{l\lambda_j} + \underline{\xi}_{t_i\lambda_j} \qquad \text{Eq. 2}$$

$$\underline{\Psi} = CE^T + \underline{\Xi} \qquad \text{Eq. 3}$$

where the $m \times n$ matrix Ψ denotes the measured time resolved spectra, measured at m time instants t_i, and n wavelengths λ_j. c_{lt_i} denotes the concentration of component l at time t_i, $\varepsilon_{l\lambda_j}$ denotes the emission of component l that occurs at wavelength λ_j, and $\underline{\xi}_{t_i\lambda_j}$ denotes a Gaussian distributed stochastic disturbance with zero mean. The c_{lt_i} and $\varepsilon_{l\lambda_j}$ are gathered in the matrices C and E, of dimension $m \times n_{\text{comp}}$ and $n \times n_{\text{comp}}$, respectively. Matrix Ξ is, like Ψ, $m \times n$.

Regarding Eq. 2 we note that the quantity which will be estimated is the product $c_l\varepsilon_l^T$ which in itself is insufficient for the determination of the absolute

[1] Notation convention: underlining indicates stochastic variables, uppercase represents matrices, lowercase represents scalars or vectors, a circumflex indicates estimator.

at least 15 minutes. For excitation of the samples at 308 nm a Labda-Physik EMG 101 Xe/HCl excimer laser was used which produces pulses with an essentially Gaussian time profile with a width of about 7 ns and a power of 5–10 mJ/pulse. The laser was operated at a rate of 2–5 Hz. Fluorescence was detected at a right angle (through a cut-off filter in some cases) and collected by an optical fibre which led to a Jarrell-Ash monospec 27 model 1234 spectrograph in which the light was dispersed by a grating (150 grooves/mm) onto an MCP intensified diode array detector (EG&G 1421G, 25 mm, 1024 diodes). With this set-up a spectral range of about 600 nm was covered with a bandwidth of 5 nm (25 μm entrance slit) or 7 nm (250 μm slit). The detector was gated with a width of 5 ns by an EG&G 1302 pulse generator. The timing of the laser and Optical Multichannel Analyser (OMA) gate pulse was controlled by the EG&G OMA III model 1460 console with a 1303 pulse delay generator and a digital delay generator (EG&G model 9650).

Each experiment involved recording spectra at 15–45 different time instants with a constant time increment, or with a gradually increasing increment. At each time point spectra from 4–10 shots were averaged. In order to allow the experiment to be extended over a sufficiently large number of laser shots, without degradation of the sample, the laser pulse power was attenuated to less than 1 mJ/pulse by means of neutral density filters. This was necessary in particular in the case of compound 3. The spectral intensities were not corrected for the wavelength dependent response of the detection system.

Steady state fluorescence spectra were recorded on a Spex Fluorolog II emission spectrometer, using an excitation wavelength of 300 nm.

Theoretical

The basic model which describes the time evolution of spectra is the following[1]:

$$\underline{\Psi}_{t_i\lambda_j} = \sum_{l=1}^{n_{\text{comp}}} c_{lt_i}\, \varepsilon_{l\lambda_j} + \underline{\xi}_{t_i\lambda_j} \qquad \text{Eq. 2}$$

$$\underline{\Psi} = CE^T + \underline{\Xi} \qquad \text{Eq. 3}$$

where the $m \times n$ matrix Ψ denotes the measured time resolved spectra, measured at m time instants t_i, and n wavelengths λ_j. c_{lt_i} denotes the concentration of component l at time t_i, $\varepsilon_{l\lambda_j}$ denotes the emission of component l that occurs at wavelength λ_j, and $\underline{\xi}_{t_i\lambda_j}$ denotes a Gaussian distributed stochastic disturbance with zero mean. The c_{lt_i} and $\varepsilon_{l\lambda_j}$ are gathered in the matrices C and E, of dimension $m \times n_{\text{comp}}$ and $n \times n_{\text{comp}}$, respectively. Matrix Ξ is, like Ψ, $m \times n$.

Regarding Eq. 2 we note that the quantity which will be estimated is the product $c_l\varepsilon_l^T$ which in itself is insufficient for the determination of the absolute

[1] Notation convention: underlining indicates stochastic variables, uppercase represents matrices, lowercase represents scalars or vectors, a circumflex indicates estimator.

zero except for its diagonal, which contains the singular values. With n_{comp} components and noise-free data we have exactly n_{comp} significant singular values: $s_1 \geq s_2 \geq \ldots \geq s_{n_{comp}} > s_{n_{comp}+1} = \ldots = 0$.

ESTIMATION OF SPECTRAL AND KINETIC PARAMETERS

Let us assume in the following that we have successfully determined n_{comp}. Unknown in Eq. 3 are the spectral parameters of the $n \times n_{comp}$ matrix E and the parameters which describe the $m \times n_{comp}$ concentration matrix C which we gather in the parameter vector θ. Now for fixed θ Eq. 3 represents a multivariate Gauss-Markoff model (Koch 1988), of which the solution is given by:

$$\underline{\hat{E}}^T(\theta) = C^{\dagger}(\theta)\,\underline{\Psi} \qquad \text{Eq. 8}$$

$C^{\dagger}$ denotes the Moore-Penrose generalized inverse of C, which is of full rank.

Following Kaufman (1975) and Golub and Leveque (1979) we perform a QR decomposition of $C(\theta)$:

$$C(\theta) = [Q_1(\theta)\; Q_2(\theta)] \begin{bmatrix} R(\theta) \\ 0 \end{bmatrix} = Q_1(\theta) R(\theta) \qquad \text{Eq. 9}$$

where $Q_1(\theta)$ and $Q_2(\theta)$ are, respectively, $m \times n_{comp}$ and $m \times (m - n_{comp})$ matrices which together form the orthogonal matrix $Q(\theta)$. $R(\theta)$ represents an $n_{comp} \times n_{comp}$ upper triangular matrix.

Combining Eq. 8 and Eq. 9 we have:

$$\underline{\hat{E}}^T(\theta) = R^{-1}(\theta)\; Q_1^T(\theta)\,\underline{\Psi} \qquad \text{Eq. 10}$$

Combining Eq. 9 and Eq. 10 we find for the residual matrix Z:

$$\underline{Z}(\theta) = \underline{\Psi} - C(\theta)\,\underline{\hat{E}}^T(\theta) = (I - Q_1(\theta)\; Q_1^T(\theta))\,\underline{\Psi} = Q_2(\theta)\; Q_2^T(\theta)\,\underline{\Psi} \qquad \text{Eq. 11}$$

where $Q_2(\theta)\; Q_2^T(\theta)$ is an orthogonal projection matrix. In situation i] the determinant to be minimized as a function of the unknown parameters θ is given by (Bates and Watts 1988)

$$\underline{Y}(\theta) = \det(\underline{Z}^T(\theta)\,\underline{Z}(\theta)) = \det(\underline{\Psi}^T Q_2(\theta)\; Q_2^T(\theta)\,\underline{\Psi}) \qquad \text{Eq. 12}$$

since $Q_2^T(\theta)\; Q_2(\theta) = I_{m-n_{comp}}$, where $I_{m-n_{comp}}$ denotes the identity matrix of dimension $m - n_{comp}$. Thus we have eliminated the linear parameters E and have arrived at a residual matrix $Q_2^T(\theta)\,\underline{\Psi}$ with $m - n_{comp}$ observations of n responses.

This leaves as degrees of freedom: $df = m - n_{comp} - n_{par}$, where $n_{par} = \dim(\theta)$. Thus when $df \leq 0$ or when $n_{obs} = m - n_{comp} < n = n_{resp}$ (Eq. 6) the multiresponse problem is unsolvable. Minimization of $\underline{Y}(\theta)$ gives us the maximum likelihood estimate $\underline{\hat{\theta}}$.

When the multiresponse problem is unsolvable it may be that situation ii] approximately applies. Anyway, we can always calculate the nonlinear least squares estimator. In situation ii] the sum of squares to be minimized as a function of the unknown parameters θ is given by

$$\underline{Y}(\theta) = \text{trace}(\underline{Z}^T(\theta)\,\underline{Z}(\theta)) = \text{trace}(\underline{\Psi}^T Q_2(\theta)\; Q_2^T(\theta)\,\underline{\Psi}) \qquad \text{Eq. 13}$$

The number of observations now is $(m - n_{comp}) \times n$ which leaves as degrees of freedom: $df = (m - n_{comp}) \times n - n_{par}$. Thus when this $df \leq 0$ the problem cannot be solved.

The approximate covariance matrices of the spectral and kinetic parameters as well as the studentized residuals were calculated according to Van Stokkum et al. (in preparation).

Theoretically studentized residuals are distributed closely to Student's t-distribution with df degrees of freedom. To check this a χ^2 goodness-of-fit test (International Mathematical and Statistical Libraries, Inc., Houston TX, routine DCHIGF) is performed.

PROJECTING THE DATA UPON THE FIRST n_{comp} RIGHT SINGULAR VECTORS

When we assume that the standard deviation of the noise is small, we can project the data $\underline{\Psi}$ upon the first n_{comp} right singular vectors, thus omitting the information represented by the non-significant singular values s_l with $l > n_{comp}$. In other words, each spectrum consisting of n wavelength points is now represented by a linear combination of the right singular vectors, with n_{comp} coefficients. When the data are obtained with an OMA, as we have done here, $n_{comp} \ll n$, so by this projection we can appreciably reduce the amount of data, which speeds up the parameter estimation considerably. In the following we will disregard the stochastic character of the first n_{comp} right singular vectors $W_{n_{comp}}$. The projection gives us

$$\underline{\Psi} W_{n_{comp}} = (\underline{US})_{m \times n_{comp}} = CE^T W_{n_{comp}} + \underline{\Xi} W^{\bullet}_{n_{comp}} \qquad \text{Eq. 14}$$

Going from Eq. 3 to Eq. 14 we have reduced our multiresponse data from $m \times n$ to $m \times n_{comp}$. Instead of E we must now estimate the $n_{comp} \times n_{comp}$ projected spectral parameters $E^T W_{n_{comp}}$. The parameter estimation is completely analogous to the unprojected case.

COMPARTMENTAL MODELS

We will consider linear compartmental models with two or three compartments. From the model function CE^T we know that only the shapes of the concentration functions can be determined. To ensure the identifiability of model parameters we restrict ourselves to models where each compartment receives only one input. This input comes either from the outside environment or from another compartment. This excludes models with back reactions. Back reactions are not present in the systems studied. In a linear compartmental model the differential equation for the concentrations is:

$$\frac{d}{dt} c(t) = Kc(t) + j(t) \qquad \text{Eq. 15}$$

where c and j are 3×1 vectors: $c = [c_1\ c_2\ c_3]^T$, $j(t) = i(t)\ [1 x_4\ x_5]^T$. $i(t)$ is the result of a convolution of the exciting laser pulse and the detector response. In the case of the present experiments $i(t)$ can be very well approximated as:

$$i(t) = \frac{1}{\tau}\left(\frac{2}{\pi}\right)^{1/2} e^{-(t-\mu)^2/(2\tau^2)} \qquad \text{Eq. 16}$$

The transfer matrix K is of lower triangular form:

$$K = \begin{bmatrix} -k_1 & 0 & 0 \\ x_1 & -k_2 & 0 \\ x_2 & x_3 & -k_3 \end{bmatrix} \qquad \text{Eq. 17}$$

We assume that all k_i are different, and that $c(-\infty) = 0$. The x_i define the model. x_1, x_2 and x_3 determine the interconversions between components, and together with x_4 and x_5 they determine whether components 2 and 3 are formed by excitation or by a reaction. With the restriction of only one input per compartment we can distinguish four cases:

$$\begin{aligned} &\text{I: } x_1 = x_2 = x_3 = 0 \quad x_4 = x_5 = 1 \\ &\text{II: } x_2 = x_3 = x_4 = 0 \quad x_1 = x_5 = 1 \\ &\text{III: } x_3 = x_4 = x_5 = 0 \quad x_1 = x_2 = 1 \\ &\text{IV: } x_2 = x_4 = x_5 = 0 \quad x_1 = x_3 = 1 \end{aligned} \qquad \text{Eq. 18}$$

In words: Model I represents three independent decays (abbreviated 1| 2| 3). In Model II component 2 is a reaction product of component 1 (1→2| 3). In Model III both component 2 and 3 are reaction products of component 1 (2←1→ 3). Finally, Model IV represents a chain where component 3 is a reaction product of component 2 which on its turn is a reaction product of component 1 (1 → 2 → 3). Note that the values of the x_i cannot be estimated, because we can only estimate the shapes of the $c_i(t)$.

The solution of Eq. 15 is given by $c(t) = e^{Kt} \oplus j(t)$ where $\oplus$ indicates convolution. For Model I we find

$$c_I^I(t, k_i, \mu, \tau) = e^{-k_i\mu} e^{k_i\left(\mu + \frac{k_i\tau^2}{2}\right)} \{1 + \operatorname{erf}\left(\frac{t - (\mu + k_i\tau^2)}{2^{1/2}\tau}\right)\} \qquad \text{Eq. 19}$$

The concentration matrix C has elements $[C_I]_{pq} = c_q^I(t_p, k_q, \mu, \tau)$. The solutions to Model II–IV are linear combinations of the c_i^I and thus transformations of C_I. Writing $C_{II} = C_I A_{II}$ and so on we find:

$$A_{II} = \begin{bmatrix} 1 & -(k_1-k_2)^{-1} & 0 \\ 0 & (k_1-k_2)^{-1} & 0 \\ 0 & 0 & 1 \end{bmatrix} \qquad A_{II}^{-1} = \begin{bmatrix} 1 & 1 & 0 \\ 0 & (k_1-k_2) & 0 \\ 0 & 0 & 1 \end{bmatrix} \qquad \text{Eq. 20}$$

$$A_{III} = \begin{bmatrix} 1 & -(k_1-k_2)^{-1} & -(k_1-k_3)^{-1} \\ 0 & (k_1-k_2)^{-1} & 0 \\ 0 & 0 & (k_1-k_3)^{-1} \end{bmatrix} \quad A_{III}^{-1} = \begin{bmatrix} 1 & 1 & 1 \\ 0 & (k_1-k_2) & 0 \\ 0 & 0 & (k_1-k_3) \end{bmatrix} \qquad \text{Eq. 21}$$

$$A_{IV} = \begin{bmatrix} 1 & -(k_1-k_2)^{-1} & (k_1-k_2)^{-1}(k_1-k_3)^{-1} \\ 0 & (k_1-k_2)^{-1} & -(k_1-k_2)^{-1}(k_2-k_3)^{-1} \\ 0 & 0 & (k_1-k_3)^{-1}(k_2-k_3)^{-1} \end{bmatrix} A_{IV}^{-1} = \begin{bmatrix} 1 & 1 & 1 \\ 0 & (k_1-k_2) & (k_1-k_3) \\ 0 & 0 & (k_1-k_3)(k_2-k_3) \end{bmatrix}$$

Eq. 22

Because we are dealing with a model function CE^T the *models I–IV will produce exactly the same residual matrix Z.* For instance:

$$\underline{\hat{E}}_{II}^T(\theta) = C_{II}^{\dagger}(\theta)\,\underline{\Psi} = (C_I(\theta)\,A_{II})^{\dagger}\,\underline{\Psi} = A_{II}^{-1}C_I^{\dagger}(\theta)\,\underline{\Psi} = A_{II}^{-1}\underline{\hat{E}}_I^T \qquad \text{Eq. 23}$$

$$\underline{Z}(\theta) = \underline{\Psi} - C_{II}(\theta)\,\underline{\hat{E}}_{II}^T(\theta) = \underline{\Psi} - C_I(\theta)\,A_{II}A_{II}^{-1}\underline{\hat{E}}_I^T(\theta) = \underline{\Psi} - C_I(\theta)\,\underline{\hat{E}}_I^T(\theta) \qquad \text{Eq. 24}$$

Thus the minimum of the criterion $Y(\theta)$ (Eq. 12, Eq. 13) is independent of the chosen model as are the estimated parameters $\theta = [k_1\ k_2\ k_3\ \mu\ \tau]^T$. From Eq. 23 we conclude that the difference between the models lies in their spectral parameters. A priori knowledge about E (for instance non-negativity of the $\varepsilon_i(\lambda)$) offers us the possibility to choose between alternative models.

STEADY STATE FLUORESCENCE SPECTRUM AND QUANTUM YIELDS

When we have estimated the rate constants we can predict the shape of the steady state fluorescence spectrum ψ_∞ which results from a constant input. We will use the subscript ∞ to indicate steady state conditions. Since $\frac{dc}{dt} = 0$ and $i(t)$ is now a constant we find $c_{i,\infty}^I = k_i^{-1}$. Thus:

$$\psi_\infty(\lambda) = \sum_{i=1}^{n_{comp}} \psi_{i,\infty}(\lambda) = \sum_{i=1}^{n_{comp}} k_i^{-1}\,\hat{\varepsilon}_i^I(\lambda) \qquad \text{Eq. 25}$$

Analogous to Eq. 24 this Eq. 25 is independent of compartmental model. E.g. with Model II we find (Eq. 20) $c_{2,\infty}^{II} = c_{1,\infty}^{II}k_2^{-1} = k_1^{-1}k_2^{-1}$. We will first consider a two-compartment Model II, and omit superscript *II*. The real concentration $\tilde{c}_2$ (where the ~indicates "real") is proportional to x_1 (defined in Eq. 17), which is equal to the product of k_1 and Φ_{12}, the fractional yield of component 2 from component 1.
We thus find

$$\frac{\tilde{c}_{2,\infty}}{\tilde{c}_{1,\infty}} = \frac{c_{2,\infty}}{c_{1,\infty}} \cdot k_1\Phi_{12} = k_2^{-1}k_1\Phi_{12} \qquad \text{Eq. 26}$$

The total fluorescence quantum yield Φ_{tot} is given by

$$\Phi_{tot} = \frac{\tilde{c}_{1,\infty}\Phi_1 + \tilde{c}_{2,\infty}\Phi_2}{\tilde{c}_{1,\infty} + \tilde{c}_{2,\infty}} = \Phi_1\left(1 + \frac{\tilde{c}_{2,\infty}\Phi_2}{\tilde{c}_{1,\infty}\Phi_1}\right) / \left(1 + \frac{\tilde{c}_{2,\infty}}{\tilde{c}_{1,\infty}}\right) \qquad \text{Eq. 27}$$

where $\Phi_i = k_{f,i}/k_i$ is the quantum yield of fluorescence of component i. Now $\tilde{c}_{i,\infty}\Phi_i$ is proportional to the contribution of component i to the steady state fluorescence spectrum integrated over the entire width of the emission band (Cantor and Schimmel 1980):

$$\tilde{c}_{i,\infty}\Phi_i = g^{-1}\int\psi_{i,\infty}d\lambda = g^{-1}\tilde{c}_{i,\infty}\int\tilde{\varepsilon}_i d\lambda = g^{-1}c_{i,\infty}\int\hat{\varepsilon}_i d\lambda \qquad \text{Eq. 28}$$

where g is the fraction of radiation actually collected by the detector. Thus we find

$$\frac{\tilde{c}_{2,\infty}\Phi_2}{\tilde{c}_{1,\infty}\Phi_1} = \frac{c_{2,\infty}\int\hat{\varepsilon}_2 d\lambda}{c_{1,\infty}\int\hat{\varepsilon}_1 d\lambda} = \frac{\int\hat{\varepsilon}_2 d\lambda}{k_2\int\hat{\varepsilon}_1 d\lambda} \qquad \text{Eq. 29}$$

In conclusion: measurement of the total fluorescence quantum yield Φ_{tot} allows us to calculate the quantum yields Φ_i through combination of Eq. 26, Eq. 27 and Eq. 29, provided we know Φ_{12}. Analysis of a three-compartment Model II is a little more difficult, since we also need to know $\tilde{c}_{3,\infty}/\tilde{c}_{1,\infty}$ in the extended version of Eq. 27.

RESULTS

We will compare nonlinear least squares (NLLS) and multiresponse (MR) fits of different compartmental models. For illustrative purposes we first describe the time-resolved spectrum of system **2** which is shown in fig. 1. From the Singular Value Decomposition of Ψ (system **2**) depicted in fig. 2 we conclude that two singular values are significantly different from the noise singular values (squares in fig. 2c). The corresponding first two singular vector pairs (fig. 2a,b) are practically noise free. Thus we conclude that we are dealing with a two-component system. The shape of the input $i(t)$ was determined from the scattered excitation light at 308 nm. The parameters μ and τ thus obtained were fixed in the ensueing analysis. From the NLLS fit rate constants corresponding to a fast (F) decay and to a slow (S) decay are found. We applied Model I (abbreviated $F|S$) and the two permutations of Model II ($F \rightarrow S$ and $S \rightarrow F$). Fig. 3a,b depict the estimated spectra $\varepsilon_i^I(\lambda)$ and $\varepsilon_i^{II,F\rightarrow S}(\lambda)$. We conclude from the partial negativity of $\varepsilon_1^I(\lambda)$ (squares in fig. 3a) that Model I results in a spectrum which violates the physical constraints, whereas Model II($F \rightarrow S$) results in nonnegative fluorescence emission spectra (fig. 3b). Model II($S \rightarrow F$) also resulted in a partly negative spectrum of the fast decaying component $\varepsilon_2^{II,S\rightarrow F}(\lambda)$ (not shown). Thus we reject Model I and Model II($S \rightarrow F$) and retain Model II($F \rightarrow S$). The residuals of the NLLS fit in fig.

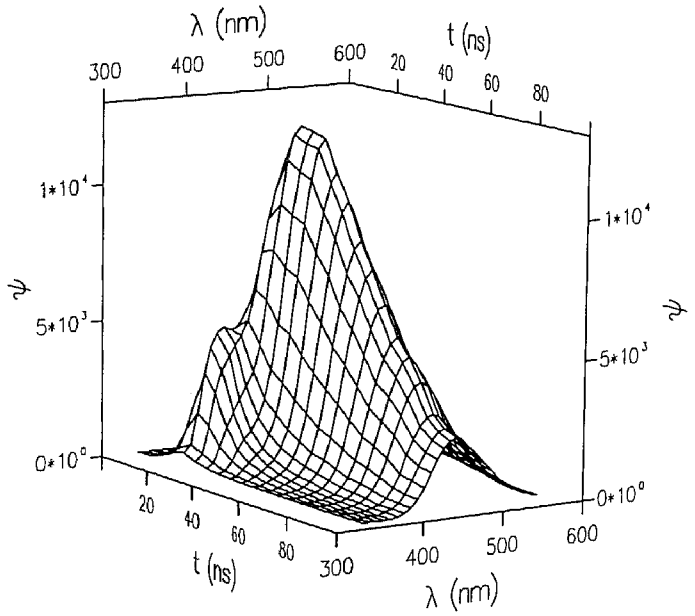

Fig. 1. Time resolved spectrum Ψ of system **2** in n-hexane.

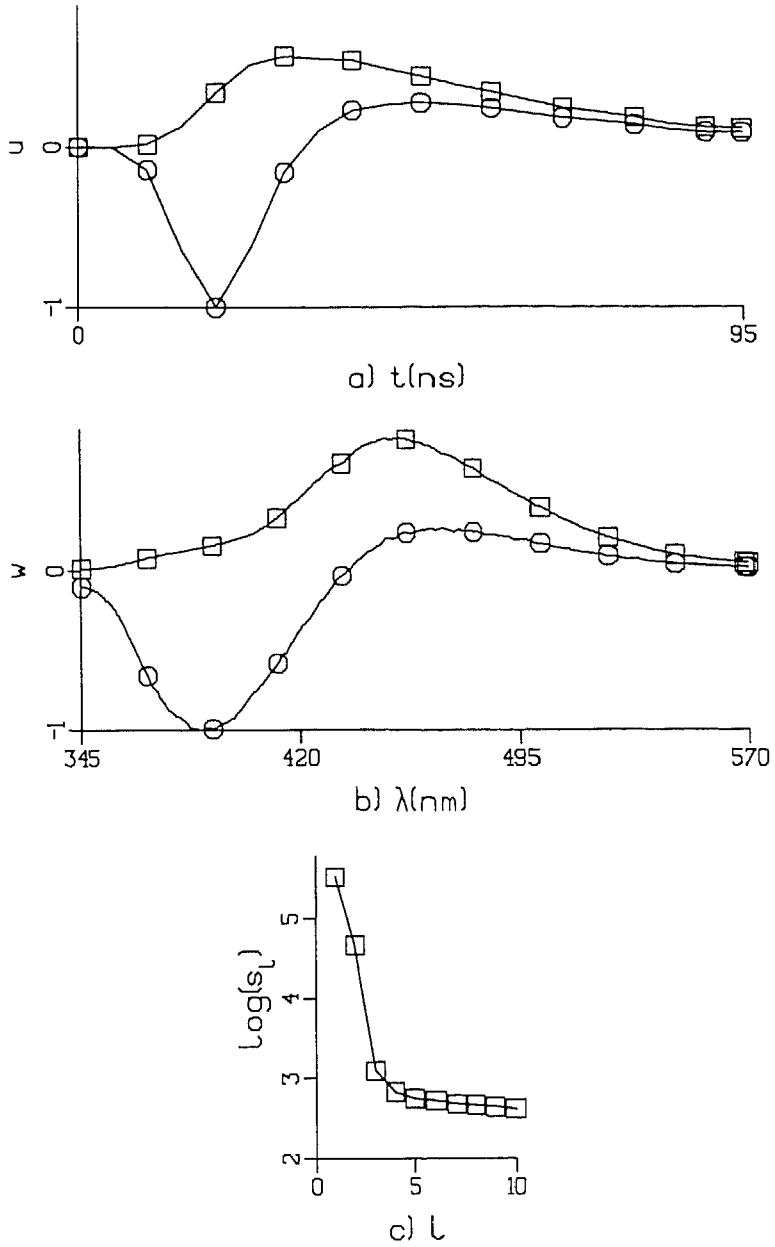

Fig. 2. Singular value decomposition of Ψ (system **2**). (a) First (squares) and second (circles) left singular vectors. (b) First (squares) and second (circles) right singular vectors. (c) Singular values one to ten on a logarithmic scale.

4 show inconstant variance. In particular a wavelength dependence appears, which resembles the spectra. This indicates that the model for the concentrations is still inadequate, e.g. because of jitter which causes concentration fluctuations. In particular near the maximum of the laser pulse small shot-to-shot variations

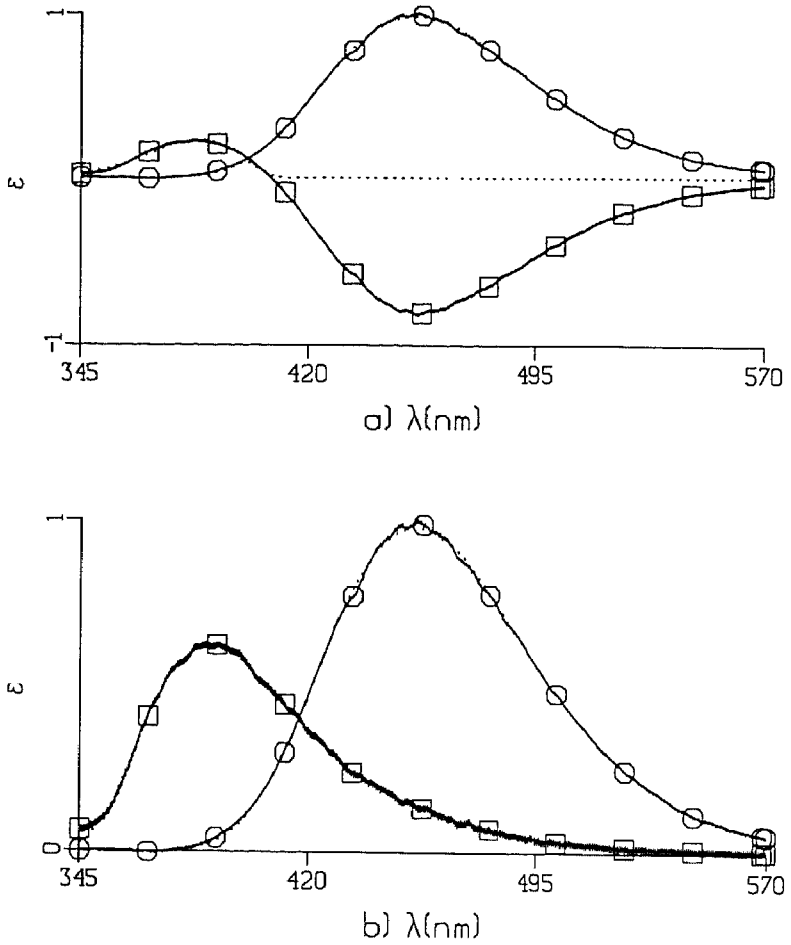

Fig. 3. Results of NLLS fit of Ψ (system 2) using Model I and Model II($F \rightarrow S$) with component one (squares) and two (circles). (a) Spectra $\varepsilon_1^I(\lambda)$ and $\varepsilon_2^I(\lambda)$. At each wavelength a vertical bar is drawn from $\hat{\varepsilon}_l - \hat{\sigma}_{\hat{\varepsilon}_l}$ to $\hat{\varepsilon}_l + \hat{\sigma}_{\hat{\varepsilon}_l}$, thus the thickness of the lines represents the uncertainty in $\hat{\varepsilon}_l$. (b) Spectra $\varepsilon_1^{II,F\rightarrow S}(\lambda)$ and $\varepsilon_2^{II,F\rightarrow S}(\lambda)$. The dotted lines represent fitted curves described in the text.

of the pulse power and of the time delay between laser pulse and gate pulse (time jitter) cause relatively large deviations of the intensities from those described by the kinetic model. At longer times, the intensities change less rapidly, and errors caused by jitter are smaller. Experience shows that the shot-to-shot intensity variations of the excimer laser are well within 10% and that under normal conditions the time jitter is less than 2 ns. In any case, the accuracy of the experiment should benefit from a fairly large number of laser shots used (typically several hundreds), provided there is no drift of laser intensity or timing, a condition normally satisfied by the equipment.

We also performed a MR fit using the data projected upon the first two right singular vectors.

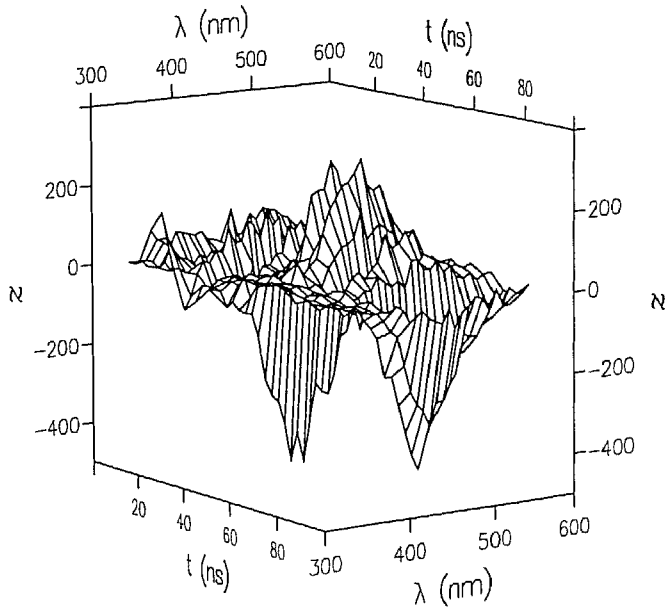

Fig. 4. Residuals of NLLS fit of Ψ (system **2**) using Model I or Model II with two components.

The residuals from this fit were acceptable and the $c_l^{II,F\rightarrow S}(t)$ and $\varepsilon_l^{II,F\rightarrow S}(\lambda)$ are shown in fig. 5. The resemblance between fig. 3b and fig. 5b indicates that the spectra are described very well by their projection upon the first two right singular vectors. Table 1 contains the estimates of the kinetic parameters from the NLLS and MR fit. We note a difference of 15% in k_1 and of 6% in k_2. From fig. 5 we predict that at wavelengths greater than 500 nm and times greater than 60 ns only one component contributes. The analysis of this restricted data set resulted in a value for k_2 close to the value estimated from the full data set using the NLLS analysis. Since only one response is fitted, NLLS and MR fit produce exactly the same estimate (column four and five of table 1).

The analysis of system **1** went analogously. Again Model II($F\rightarrow S$) was chosen because Model I produced a partly negative spectrum $\varepsilon_l^I(\lambda)$. The residuals of the NLLS fit were wavelength dependent, whereas the MR fit was satisfactory. The $c_l^{II,F\rightarrow S}(t)$ and $\varepsilon_l^{II,F\rightarrow S}(\lambda)$ are depicted in fig. 6. The decays of system **1** (Fig. 6a) are faster than those of system **2** (fig. 5a). The spectra of system **1** (fig. 6b) are blue-shifted relative to the spectra of system **2** (fig. 5b).

The shape of a charge transfer fluorescence emission spectrum is often well described by a Gaussian in the energy domain (Marcus 1989):

$f(\bar{\nu})/\bar{\nu}^3 = f_{max}\exp(-\ln 2[2(\bar{\nu} - \bar{\nu}_{max})/\Delta\bar{\nu}]^2)$ where $\bar{\nu} = \lambda^{-1}$ denotes the wavenumber and $f(\bar{\nu})$ is the converted fluorescence emission spectrum: $f(\bar{\nu}) = \lambda^2\varepsilon(\lambda)$ (Lakowicz 1983). Even better fits are achieved when an extra skewness parameter is introduced (Fraser and Suzuki 1969; Sevilla et al. 1989). Thus we arrive at the model function

$$\varepsilon(\bar{\nu}) = \bar{\nu}^5 f_{max}\exp(-\ln 2[\ln(1 + 2b(\bar{\nu} - \bar{\nu}_{max})/\Delta\bar{\nu})/b]^2) \qquad \text{Eq. 30}$$

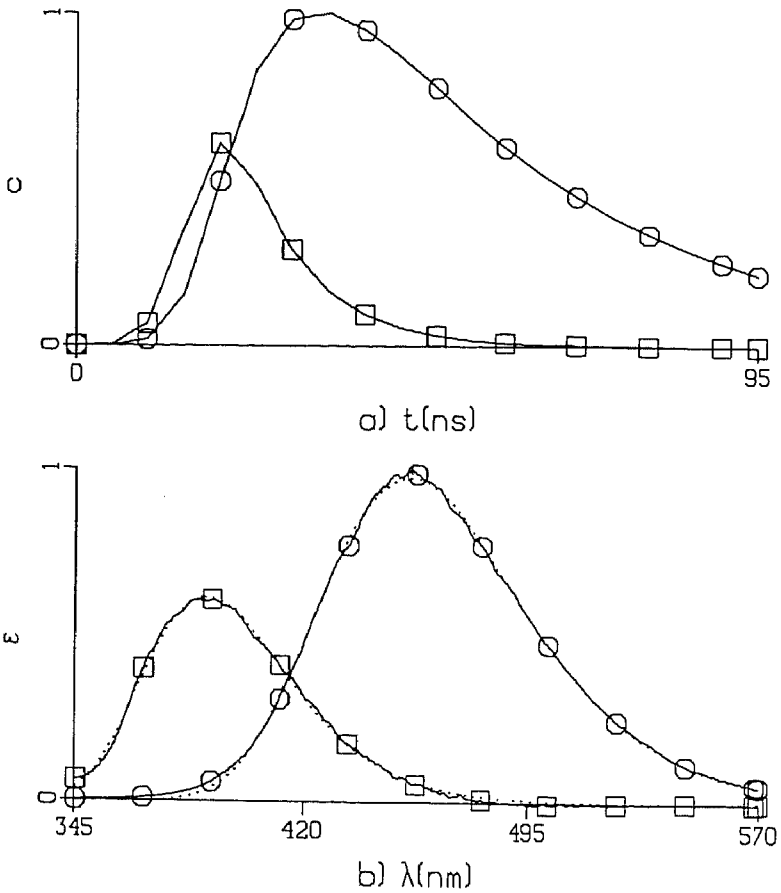

Fig. 5. Results of MR fit of Ψ (system 2) using Model II($F \rightarrow S$) with component one (squares) and two (circles). Since the product $c\varepsilon^T$ is estimated, we calculate the extremum of this product per component, and scale according to the maximum of the extrema of all components. Here we have max $(c_1\varepsilon_1^T) = (0.6)^2$max $(c_2\varepsilon_2^T)$. The curves are thus scaled according to their contribution to Ψ. (a) Concentrations $c_1^{II}(t)$ and $c_2^{II}(t)$. (b) Spectra $\varepsilon_1^{II}(\lambda)$ and $\varepsilon_2^{II}(\lambda)$. At the maxima a vertical line is drawn which indicates the estimated standard error in $\hat{\varepsilon}_i$. The dotted lines represent fitted curves described in the text.

Table 1. Estimates of kinetic model parameters of system 2 in n-hexane. Column two, three: results from NLLS and MR fit using the full data set. In columns four and five the restricted data set was used. The MR fits in columns three and five result from the analysis of the data projected upon the first two, respectively first, right singular vectors.

parameter	345–570 nm, 95 ns NLLS	MR	500–570 nm, 65–95 ns NLLS	MR
k_1	0.096	0.113		
k_2	0.032	0.030	0.032	0.032

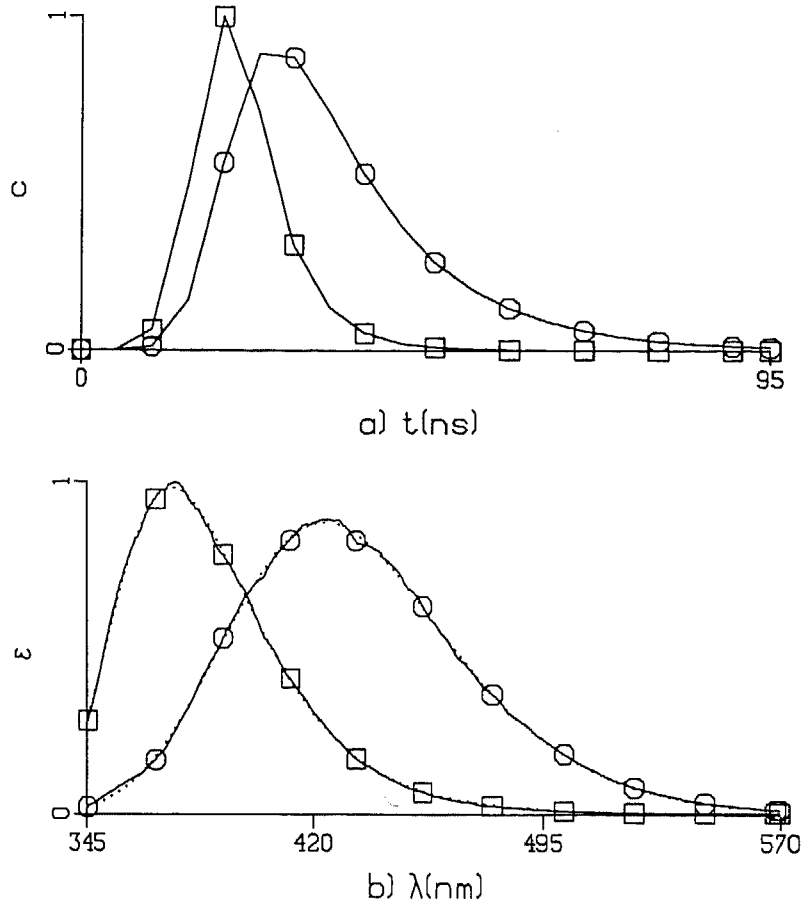

Fig. 6. Results of MR fit of Ψ (system **1**) in n-hexane using Model II($F \rightarrow S$). Layout as in fig. 5.

Note that with skewness parameter $b = 0$ the exponent in Eq. 30 reduces to a Gaussian. The maximum of Eq. 30 in the wavelength domain is given by the numerical solution of the nonlinear equation $\frac{d}{d\bar{\nu}} \varepsilon(\bar{\nu}) = 0$.

The results of this fit are represented by the dotted lines in fig. 5b and fig. 6b. This simple model function fits the spectra remarkably well.

The time-resolved spectrum of system **3** is shown in fig. 7. From the Singular Value Decomposition of Ψ (system **3**) depicted in fig. 8 we conclude that three singular values are significantly different from the noise singular values (squares in fig. 8c). The corresponding first three singular vector pairs (fig. 8a,b) are practically noise free, except perhaps for the third right singular vector (triangles in fig. 8b). Thus we conclude that we are dealing with a three-component system.

In this experiment the scattered laser light at 308 nm was removed using a cut-off filter. This enabled us to monitor the fluorescence of system **3** at wavelengths longer than 600 nm without disturbance from the excitation light transmitted in second order at 616 nm. The small price we pay for this is the estima-

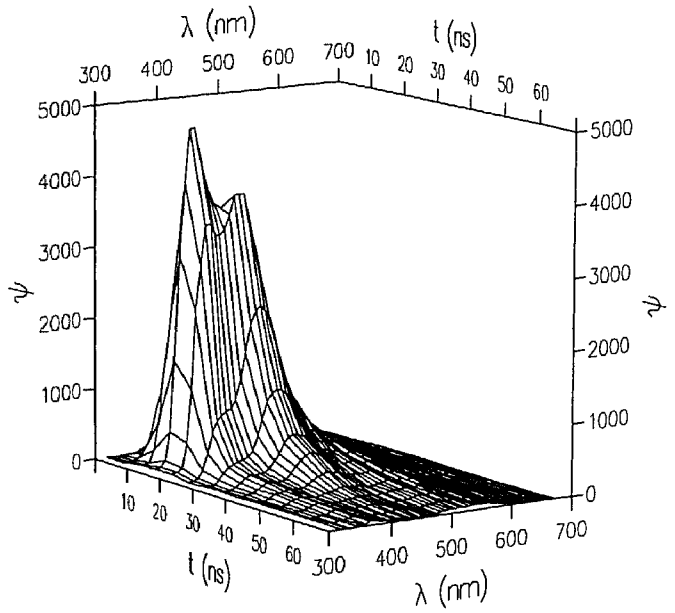

Fig. 7. Time resolved spectrum Ψ of system 3 in t-decalin.

tion of the $i(t)$ parameters (μ and τ, see Eq. 16) simultaneously with the kinetic parameters.

The NLLS fit resulted in three distinct rate constants, see column two of table 2, which we abbreviate medium (M), slow (S) and fast (F). We applied all sixteen different combinations of models and rate constants: Model I (abbreviated $F|M|S$), Model II ($M\rightarrow S|F, S\rightarrow M|F, F\rightarrow M|S, M\rightarrow F|S, F\rightarrow S|M, S\rightarrow F|M$), Model III ($M\leftarrow F\rightarrow S, F\leftarrow M\rightarrow S, F\leftarrow S\rightarrow M$) and Model IV ($F\rightarrow M\rightarrow S, F\rightarrow S\rightarrow M, M\rightarrow F\rightarrow S, M\rightarrow S\rightarrow F, S\rightarrow F\rightarrow M, S\rightarrow M\rightarrow F$). Fig. 9a,b show the spectra $\varepsilon_i^I(\lambda)$ and $\varepsilon_i^{II,M\rightarrow S|F}(\lambda)$ estimated from the NLLS fit. We note that with Model I the spectrum $\varepsilon_1^I(\lambda)$ (squares in fig. 9a) contains a small negative part around 580 nm, whereas Model II ($M\rightarrow S|F$) results in a nonnegative fluorescence emission spectrum $\varepsilon_1^{II,M\rightarrow S|F}(\lambda)$ (squares in fig. 9b). From the other fourteen combinations the results of Model IV ($F\rightarrow M\rightarrow S$) resemble Model II ($M\rightarrow S|F$), whereas Model II ($F\rightarrow M|S$, $F\rightarrow S|M$) and Model III ($M\leftarrow F\rightarrow S$) resemble Model I. All other combinations, which contain reactions where a slower decaying component reacts to a faster decaying component, produced one or more clearly unphysical spectra with large negative parts and therefore these ten models could be rejected.

The residuals of the NLLS fit which are shown in Fig. 10 are again wavelength dependent. We performed a MR fit using the data projected upon the first three right singular vectors. The residuals from this fit were acceptable and the $c_i^I(t)$ and $\varepsilon_i^I(\lambda)$ are depicted in fig. 11. Note that the small negativity of $\varepsilon_1^I(\lambda)$ around 580 nm is no longer present (compare the squares in fig. 9a and fig. 11b). The kinetic parameters estimated in the NLLS and MR fit are summarized in table 2. Comparing columns two and three we note an appreciable difference in k_2, the slowest decay rate constant.

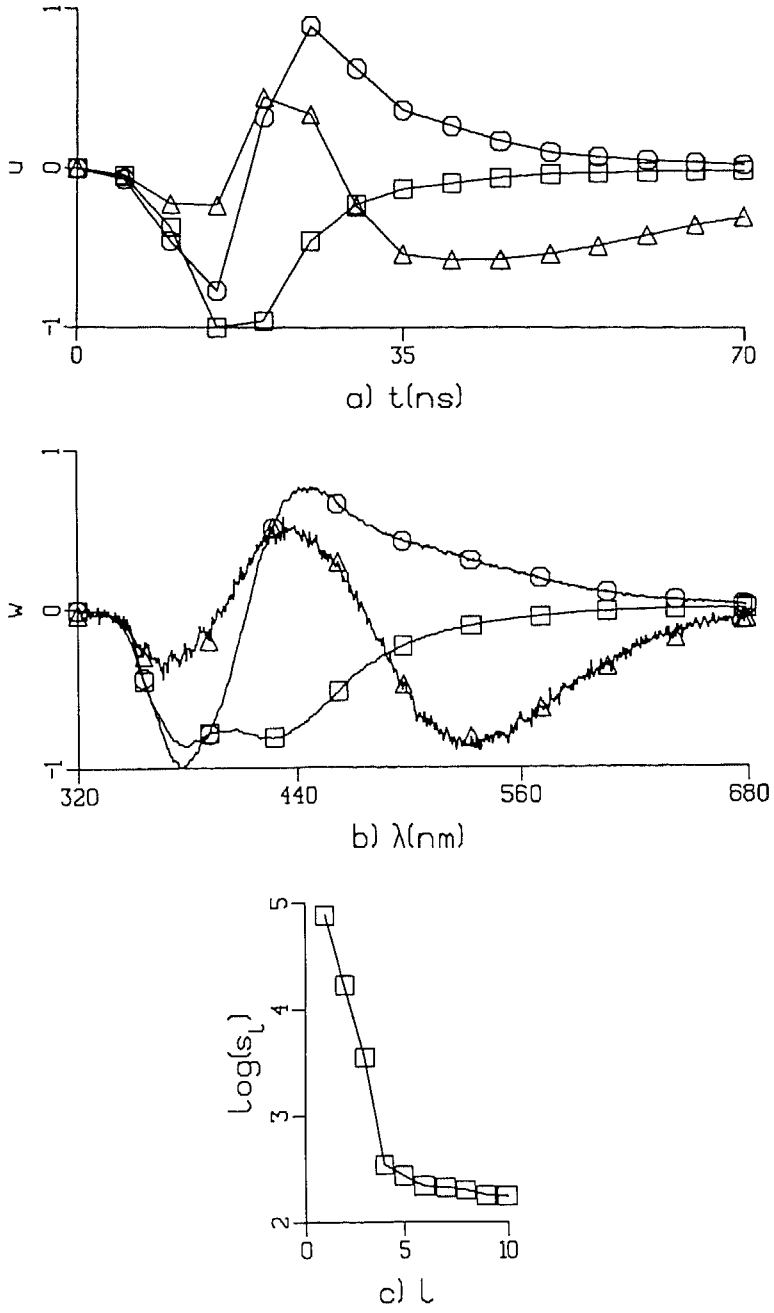

Fig. 8. Singular value decomposition of Ψ (system 3). Layout as in Fig. 2, triangles indicate third singular vectors.

From the estimated spectra in fig. 11b we predict that at wavelengths greater than 500 nm only two components contribute. This was confirmed by the SVD analysis (not shown). The kinetic parameters from the NLLS and MR fit estima-

Table 2. Estimates of kinetic model parameters of system 3 in t-decalin. Column two, three: results from NLLS and MR fit using the full data set. In columns four and five the restricted data set was used. The MR fits in columns three and five result from the analysis of the data projected upon the first three, respectively two, right singular vectors.

parameter	320–680 nm NLLS	MR	500–680 nm NLLS	MR
k_1	0.1510	0.149	0.140	0.15
k_2	0.0438	0.035	0.0363	0.034
k_3	1.150	1.10		
μ	15.19	15.08	15.14	15.4
τ	4.416	4.37	4.35	4.5
ς	17.6		7.9	

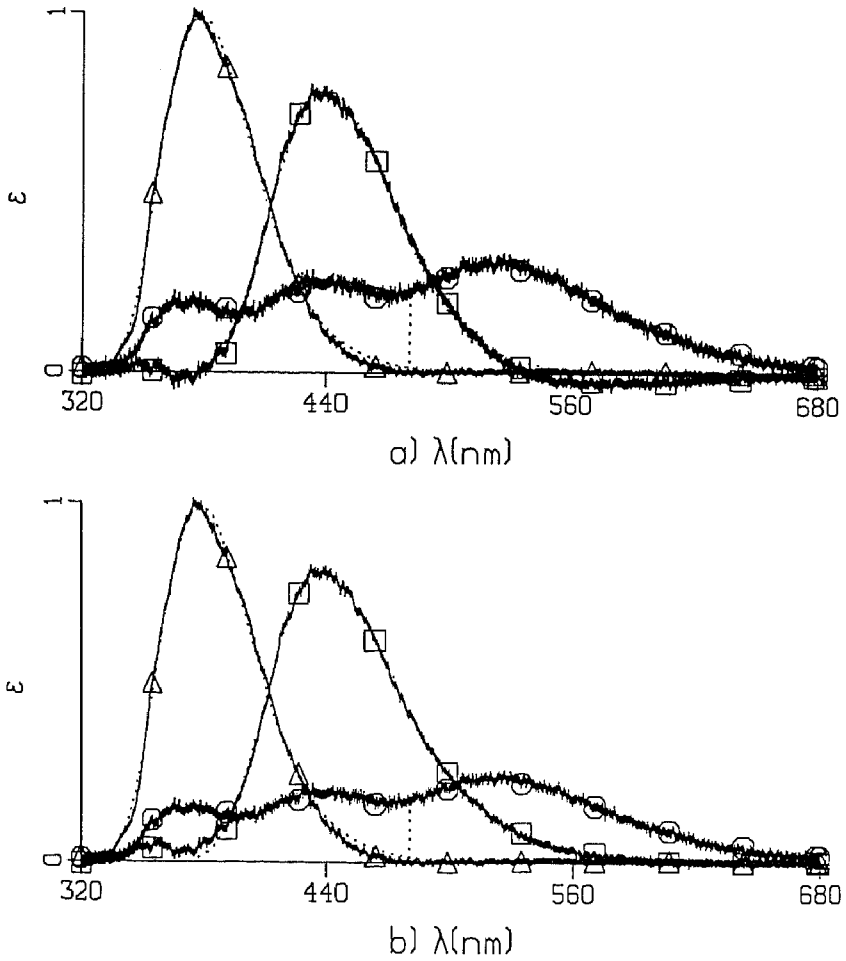

Fig. 9. Results of NLLS fit of Ψ (system 3) using (a) Model I and (b) Model II($M \rightarrow S|F$) with component one (squares), two (circles) and three (triangles). Layout as in fig. 3.

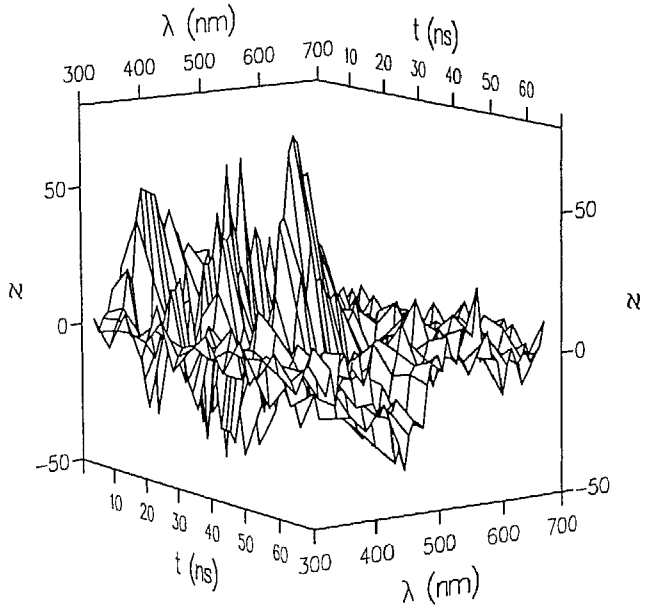

Fig. 10. Residuals of NLLS fit of Ψ (system 3).

ted from the restricted data are gathered in columns four and five of table 2. We note that k_2 obtained from these fits was about the same as the k_2 obtained from the MR fit using the full data set. We conclude that the parameters of column three of table 2 and of fig. 11b describe the complete data set satisfactorily. Again the spectra $\varepsilon_i^I(\lambda)$ estimated from the MR fit could be well fitted with the spectral model function of Eq. 30, viz. the dotted lines in fig. 11b. The $\varepsilon_i(\lambda)$ of the five alternative models which produced nonnegative spectra (Model II ($F \rightarrow M|S$, $F \rightarrow S|M$, $M \rightarrow S|F$), Model III ($M \leftarrow F \rightarrow S$), Model IV ($F \rightarrow M \rightarrow S$) could also be well fitted. The discrepancy between the F spectrum and its fit around 450 nm (triangles in fig. 11b) was smaller in models involving a reaction $F \rightarrow M$.

Table 3. Final estimates of kinetic and spectral model parameters (from multiresponse parameter estimation). Spectra were fitted according to Eq. 30. Wavenumbers $\bar{\nu}$ in 10^3 cm^{-1}; *: fit restricted to wavelengths greater than 480 nm.

model	k 10^9 s^{-1}	$\bar{\nu}_{max}$	$\Delta\bar{\nu}$	b	λ_{max} nm
system 1	0.17 ± 0.03	26.24	4.40	−0.297	373
$F \rightarrow S$	0.08 ± 0.01	22.67	4.91	−0.015	425
system 2	0.11 ± 0.03	25.24	3.97	−0.152	388
$F \rightarrow S$	0.032 ± 0.003	21.34	4.09	−0.119	455
system 3	1.0 ± 0.8	25.88	3.84	−0.147	379
$M \rightarrow S \mid F$	0.14 ± 0.02	22.12	4.32	−0.185	439
	0.032 ± 0.003	17.79*	4.54*	0.00*	533**

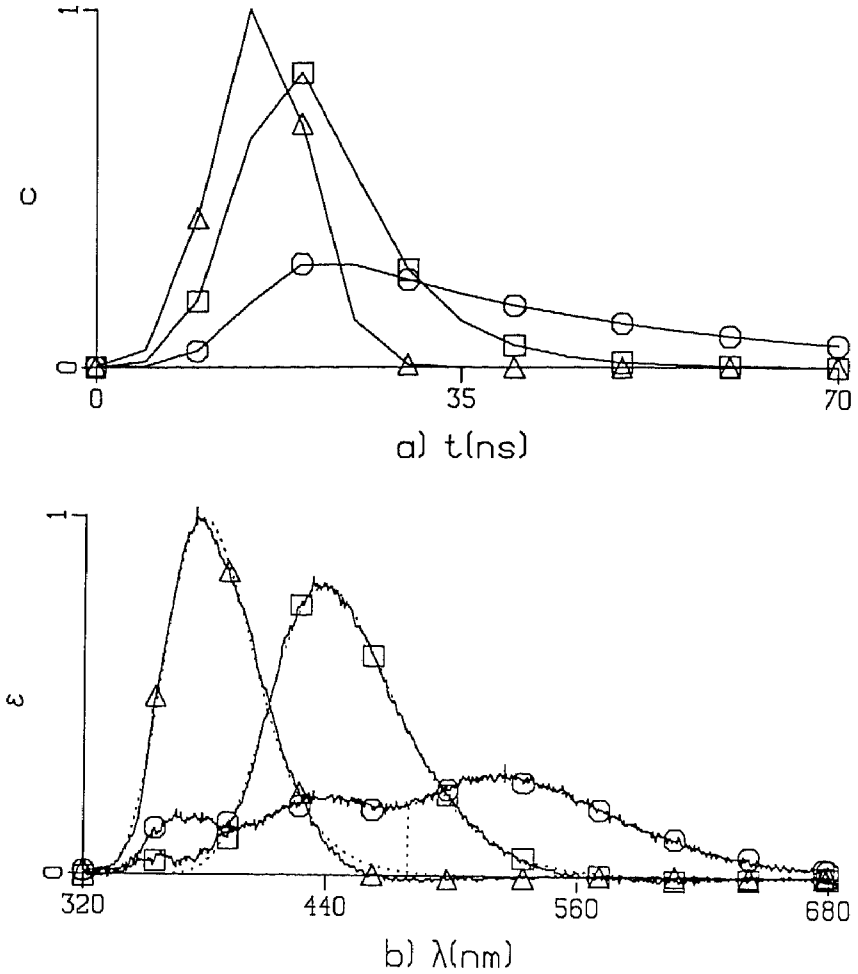

Fig. 11. Results of MR fit of Ψ (system 3) using Model I. Layout as in Fig. 5. With the smallest spectrum (circles in (b)) the fit (dotted line) was restricted to wavelengths greater than 480 nm.

The experiments were repeated at least three times and the results proved reproducable. The final estimates of the rate constants and of the fits of the spectral parameters are gathered in table 3. The shape of the steady state fluorescence spectrum observed with the spectrometer agreed well with the prediction according to Eq. 25. Therefore we refrained from a correction for the spectral response of the OMA system. Combination of the results of table 3 with the measurement of the total fluorescence quantum yield Φ_{tot} results in the quantum yields and radiative rate constants gathered in table 4. We thereby assumed Model II($M \rightarrow S|F$) for system **3** and a quantum yield for formation of component 2 $\Phi_{12} = 0.89$ which was calculated in (Brouwer et al. 1991b). Furthermore we assumed $\tilde{c}_{3,\infty}/\tilde{c}_{1,\infty} = 0.1$, i.e. the fast decaying component is formed less than the medium decaying component. With system **1** and system **2** it is assumed that $\Phi_{12} = 0.98$, extrapolating from the quantum yield of **3** in n-hexane calculated in (Brouwer et al. 1991b).

DISCUSSION

A common finding from the analysis of the behavior of system **1** and system **2** is that a species emitting at a shorter wavelength is converted on a timescale of about 10 ns to a second species emitting at a longer wavelength. An independent model described system **3** adequately, although more complex models with a conversion could not be excluded. Additional results from single-wavelength time-resolved fluorescence measurements with a better time resolution indicate that the correct model to describe system **3** should involve a step $M \rightarrow S$, which leaves only two models: $M \rightarrow S|F$ and $F \rightarrow M \rightarrow S$. Distinction between these two will require experiments with a better time resolution in view of the very short decay time of the *F*-component.

For the case of system **3** we have previously ascribed the emission bands centered at 439 and 522 nm to two different conformations of charge-transfer excited states (Brouwer et al. 1991a,b), in analogy with results from other studies on semi-flexible compounds (Gust et al. 1991). The two emission bands of system **1** and system **2** can likewise be ascribed to fluorescence from charge-transfer excited states (fig. 12). In both cases the fluorescence of the locally excited donor or acceptor chromophore is expected to occur at significantly shorter wavelengths (cf. 334 nm for 1-cyano-4-methylnaphthalene; 333 nm for 1-phenylpiperidine (Krijnen 1990)). The absence of such emission bands indicates that electron transfer occurs quantitatively in these compounds. In system **3** some local emission is observed at 377 nm.

The wavenumbers of the short-wavelength emission maxima of **1** and **2** fit well in a solvatochromic shift analysis including the maxima in more polar solvents, from which dipole moments are derived of about 29 D for both **1** and **2** (Scherer et al. to be published). These dipole moments correspond to charge separation in an extended conformation like that of the ground state. Again in line with our earlier work we ascribe the long-wavelength bands of **1** and **2** to "folded' exciplex-type conformations, the driving force for the interconversion being the elec-

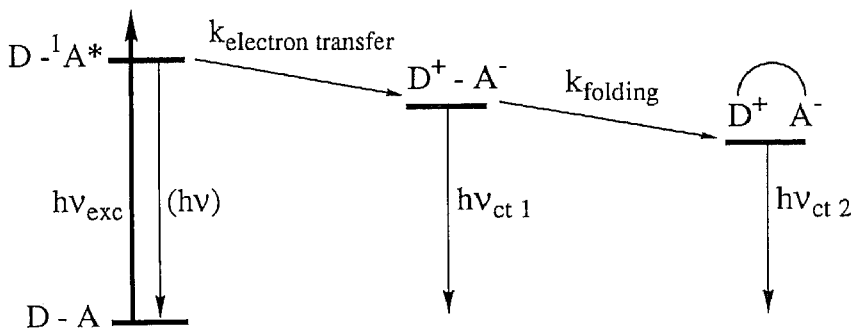

Fig. 12. Proposed common reaction scheme for the systems studied. With system **1** and system **2** fluorescence of a locally excited $D - {}^1A^*$ state is absent (indicated by the parentheses), whereas with system **3** it corresponds to the *F*-component $h\nu_{ct\,1}$ and $h\nu_{ct\,2}$ correspond to fluorescence of the extended and folded conformation respectively.

trostatic attraction between the charged D^+ and A^- groups. The difference in the band positions, 3.6×10^3 cm^{-1} for system **1**, 3.9×10^3 cm^{-1} for system **2** (see column three of table 3), corresponds roughly to the electrostatic energy gain minus the loss of solvation energy. The net energy gain of some 8 kcal/mole in n-hexane is probably big enough to compensate for the increased steric energy in the folded conformation. In going to a slightly more polar solvent this energy gain rapidly falls off, which explains why this type of dual emission is only observed in saturated hydrocarbon solvents.

Comparing the positions of the two CT-bands of system **1** and system **2** we note that the bridgehead cyano group in **2** exerts a stabilizing effect on the CT-states of as much as 1000–1500 cm^{-1} (column three of table 3). Interestingly, AM1/UHF[2] (Dewar et al. 1985) calculations predict a stabilization of the 1-cyano-4-cyclohexylnaphthalene radical anion by the additional cyano group, and show that this occurs without significant charge transfer, so that the effect may be ascribed to a charge-dipole interaction. In order to obtain a reasonable molecular model for the charge-transfer states of compound **1** we computed the structure and charges of the anilinium radical cation and the cyanonaphthalene radical anion fragments using AM1/UHF. The fragments were linked by a bridge described by the Tripos molecular mechanics force field (Sybyl version 5.32, Tripos Associates, St. Louis, Missouri, USA), and subsequently kept fixed in energy minimizations (including electrostatics with a dielectric constant of 2) starting from different bridge conformations. The resulting structures of the extended and folded CT-states are shown in fig. 13. In the folded species, in which the piperidine ring adopts a boat-like conformation, an almost ideal exciplex-like parallel orientation of the aromatic rings is possible, with an inter-ring distance of about 3 Å.

The radiative rate constants of the extended and folded CT-species reveal differences. In system **1** and system **2** the rate constants of the exciplex fluorescence are approximately equal to the k_f of the through-bond mediated emission in the extended conformation (column five of table 4). Assuming Model II ($M \rightarrow S|F$) in system **3** the extended CT-emission is clearly more effective than the exciplex-type fluorescence. Probably $k_{f,2}$ is small in system **3** because the interaction between the aromatic moieties in the folded conformer is not very favorable in spite of their close proximity (cf. fig. 4 in Brouwer et al. 1991b).

For system **1** and system **2** the analysis demonstrates unequivocally that interconversion occurs of the species emitting at short wavelength to the one emitting at longer wavelength.

The rate of this process can only be determined when the contributions to the overall rate constant of excited state decay and the conformational process can be separated. Variable temperature measurements and time-resolved microwave conductivity experiments are in progress to elucidate this point and determine Φ_{12}. Furthermore, the effects of vicosity and of the dielectric constant of the alkane solvent are under investigation.

---

[2] MOPAC 5.0 was used: J.J.P. Stewart, QCPE program 455.

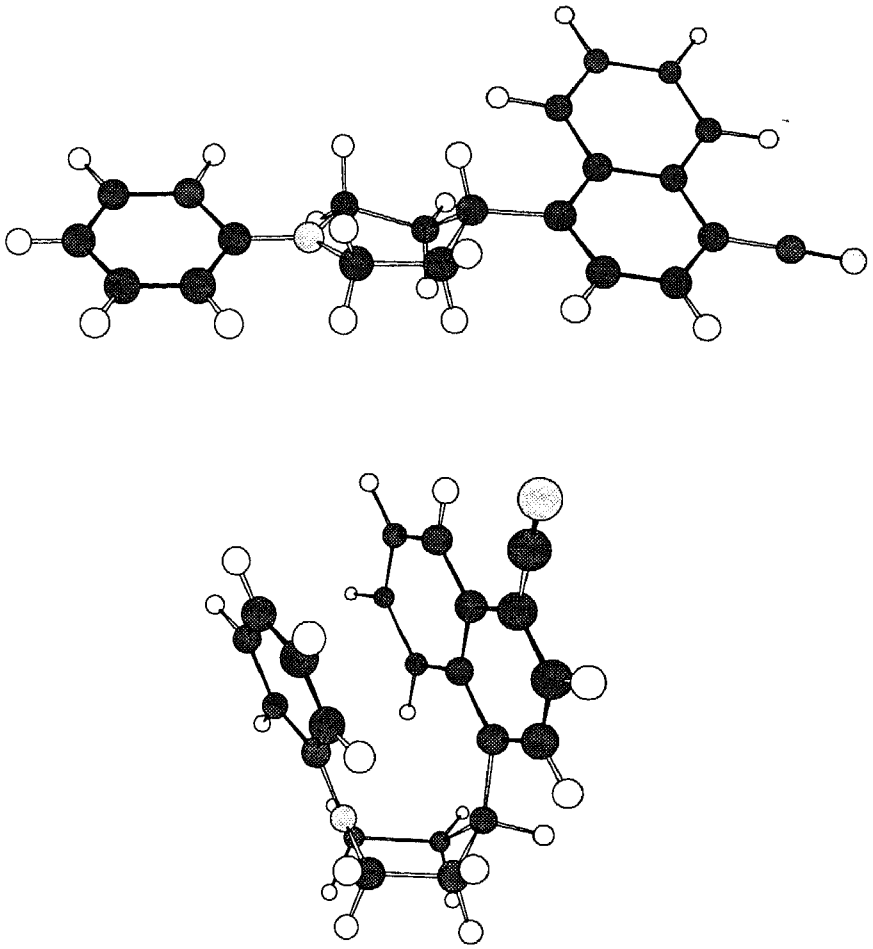

Fig. 13. Molecular models of extended and folded CT-states of compound **1** derived using molecular mechanics with AM1/UHF atomic charges. Further explanation in text.

Table 4. Quantum yields of fluorescence and estimated fluorescence rate constants. With system **1** and system **2** it is assumed that $\Phi_{12} = 0.98$. With system **3** $\Phi_{12} = 0.89$ (6) and it is assumed that $\tilde{c}_{3,\infty}/\tilde{c}_{1,\infty} = 0.1$.

model	Φ_{tot}	$k\ 10^9\ s^{-1}$	Φ	$k_f\ 10^6\ s^{-1}$
system **1**	0.07	0.17 ± 0.03	0.07	12
$F \rightarrow S$		0.08 ± 0.01	0.07	6
system **2**	0.18	0.11 ± 0.03	0.07	8
$F \rightarrow S$		0.032 ± 0.003	0.21	6
system **3**	0.01	0.14 ± 0.02	0.02	3
$M \rightarrow S \mid F$		0.032 ± 0.003	0.003	0.1
		1.0 ± 0.8	0.1	1×10^2

The fits of the spectral parameters using the model function of Eq. 30 were satisfactory (fig. 5b, fig. 6b, fig. 11b). The spectrum $\varepsilon_2'(\lambda)$ (circles in fig. 11b) contains some humps at wavelengths smaller than 480 nm. These humps coincide with the peaks of the spectra of the other two components, and are ascribed to corruption with the other spectra.

The widths of the spectra were all between 4×10^3 and 5×10^3 cm^{-1} (see column four of table 3). This agrees well with the widths of charge recombination spectra in table II of Marcus (1989).

We found that the Singular Value Decomposition performs very well, allowing a multiresponse fit with data projected upon the first n_{comp} right singular vectors.

Determination of the number of components appeared to be no problem. The results of the NLLS fits often were unsatisfactory (fig. 4, fig. 10), especially because of the large and structured residuals. The residuals resembled the spectral shapes and are caused by concentration fluctuations. These are most likely due to the jitter in the experimental set-up. We performed simulations using the estimated parameters of system **3** and a normally distributed time jitter with $\sigma = 0.5$ ns. The residuals from an NLLS fit of these simulated data were comparable to fig. 10.

We found that the MR fit (with data projected upon the first n_{comp} right singular vectors) often enabled to correct for the structured residuals. When the structured residuals are present during an appreciable fraction of the time, the assumption of a spectral covariance matrix makes sense. In this way an appropriate weighting is applied to the residuals, which prevents the large residuals domination which is present in the NLLS fit.

In the NLLS fit the slowest decaying component of system **3**, with the smallest contribution to Ψ, was estimated wrongly, which was clearly demonstrated (column two versus columns 3–5 of table 2). Using the full data set the MR fit estimated the kinetics of this small component correctly, whereas the NLLS fit resulted in a k_2-value which was 25% too large. With system **2**, columns 2–4 of table 1 are about the same.

Rejection of models is possible only on the basis of their estimated spectra. This stresses the paramount importance of gathering spectral information (e.g. by means of a multichannel spectral analyser) when studying a kinetic system. Assuming the model is right, the complete spectra of the components can be estimated with a reasonably small error, as indicated by the small vertical error bars in the plots of the spectral parameters.

Model I, which featured independently decaying components, could be rejected with system **2** and with system **1**. Only Model II($F \rightarrow S$) resulted in nonnegative fluorescence emission spectra. With system **3** out of sixteen different combinations of rate constants and models only six resulted in nonnegative spectra. More information regarding the spectra and experiments with a better time resolution are necessary to distinguish between these six models. In particular, incorporation of a priori spectral information can lead to constrained NLLS or MR model fitting. Further developments of the tools presented here will include optimiza-

tion of the experimental procedure using the OMA, and application of the method of analysis to other types of time-resolved data (e.g. transient absorption).

ACKNOWLEDGEMENTS

Drs. F.C.A. Groen, H.J.W. Spoelder, J.W. Verhoeven and J.M. Warman are thanked for critical reading of the text and inspiring discussions. E.P.M. Corten assisted with the programming. R.D. Mout and P.H. Maassen van den Brink are thanked for their contribution to the experiments.

REFERENCES

Anderson, D.H. *Compartmental modeling and tracer kinetics.* Springer: Berlin, 1983.

Andriessen, R., N. Boens, M. Ameloot, F.C. De Schryver. Non a priori analysis of fluorescence decay surfaces of excited-state processes. 2. Intermolecular excimer formation of pyrene. *J. Phys. Chem.* **95**, 2047, 1991.

Bates, D.M., D.G. Watts. *Nonlinear regression and its applications*; Wiley: New York, 1988.

Beechem, J.M., M. Ameloot, L. Brand. Global analysis of fluorescence decay surfaces: Excited-state reactions. *Chem. Phys. Lett.* **120**, 466, 1985.

Brouwer, A.M., R.D. Mout, P.H. Maassen van den Brink, H.J. Van Ramesdonk, J.W. Verhoeven, J.M. Warman, S.A. Jonker. Charge separation in the excited state of electron donor-acceptor compounds containing the piperazine moiety. *Chem. Phys. Lett.* **180**, 556, 1991.

Brouwer, A.M., R.D. Mout, P.H. Maassen van den Brink, H.J. Van Ramesdonk, J.W. Verhoeven, S.A. Jonker, J.M. Warman. Electrostatically driven folding following light-induced intramolecular electron transfer in a trichromophoric electron donor-acceptor molecule. *Chem. Phys. Lett.* **186**, 481, 1991.

Cantor, C.R., P.R. Schimmel. *Biophysical Chemistry, Part II: Techniques for the study of biological structure and function*; Freeman: New York, 1980; Chapter 8.

Cundall, R.B., R.E. Dale, Eds. *Time-resolved fluorescence spectroscopy in biochemistry and biology*; NATO ASI Series A: Life Sciences; Plenum Press: New York, 1983; Vol. 69.

Dewar, M.J.S., E.G. Zoebisch, E.F. Healy, J.J.P. Stewart. AM1: A new general purpose quantum mechanical molecular model. *J. Am. Chem. Soc.* **107**, 3902, 1985.

Fraser, R.D.B., E. Suzuki. Resolution of overlapping bands: functions for simulating band shapes. *Anal. Chem.* **41**, 37, 1969.

Godfrey, K. *Compartmental models and their application.* Academic Press: London, 1983.

Golub, G.H., R.J. LeVeque. Extensions and uses of the variable projection algorithm for solving nonlinear least squares problems. *Proc. of the 1979 Army Numerical Analysis and Comp. Conf.*, 1979, ARO Report **79-3**, 1, 1979.

Gust, D., T.A. Moore, A.L. Moore, F. Gao, D. Luttrull, J.M. DeGraziano, X.C. Ma, L.R. Makings, S.-J. Lee, T.T. Trier, E. Bittersmann, G.R. Seely, S. Woodward, R.V. Bensasson, M. Rougée, F.C. De Schryver, M. Van der Auweraer. Long-lived photoinitiated charge separation in carotene-diporphyrin triad molecules. *J. Am. Chem. Soc.* **113**, 3638, 1991.

Kaufman, L. A variable projection method for solving separable nonlinear least squares problems. *BIT*, **15**, 49, 1975.

Koch, K.-R. *Parameter estimation and hypothesis testing in linear models*; Springer: Berlin, 1988.

Krijnen, B. Through-Bond Donor-Acceptor Interaction. Structural and Conformational Effects. *Ph.D. thesis*, University of Amsterdam, 1990.

Lakowicz, J.R. *Principles of fluorescence spectroscopy*. Plenum Press: New York, 1983; Chapter 2.

Löfroth, J.E. Deconvolution of single photon counting data with a reference method and global analysis. *Eur. Biophys. J.* **13**, 45, 1985.

Marcus, R.A. Relation between charge transfer absorption and fluorescence spectra and the inverted region. *J. Phys. Chem.* **93**, 3078, 1989.

Nagle, J.F. Solving complex photocycle kinetics. Theory and direct method. *Biophys. J.*, **59**, 476, 1991.

Norrish, R.G.W., G. Porter. Chemical reactions produced by very high light intensities. *Nature*, **164**, 658, 1949.

Perrin, D.D., W.L.F. Armarego, D.R. Perrin. *Purification of laboratory chemicals*, 2nd ed.; Pergamon: Oxford, 1980.

Porter, G. Flash photolysis and spectroscopy. A new method for the study of free-radical reactions. *Proc. R. Soc. A*, **200**, 284, 1950.

Scherer, T., R.J. Willemse, J.W. Verhoeven. Comparison of flexibly and rigidly bridged donor-acceptor systems; solvent induced switching between folded and extended emissive charge-transfer states. *Recl. Trav. Chim. Pays-Bas*, **110**, 95, 1991.

Scherer, T., R.J. Willemse, J.W. Verhoeven. To be published.

Sevilla, J.M., M. Dominguez, F. Garcia-Blanco, M. Blazquez. Resolution of absorption spectra. *Computers chem.* **13**, 197, 1989.

Solar, S., W. Solar, N. Getoff. Resolved multisite OH-attack on aqueous tryptophan studied by pulse radiolysis. *Radiat. Phys. Chem.* **23**, 371, 1984.

Visscher, K.J., M.L. Hom, H. Loman, H.J.W. Spoelder, J.B. Verberne. Spectral and kinetic properties of intermediates induced by reaction of hydrated electrons with adenine, adenosine, adenylic acid and polyadenylic acid; a multi component analysis. *Rad. Phys. Chem.* **32**, 465, 1988.

Wegewijs, B., R.M. Hermant, J.W. Verhoeven, A.G.M. Kunst, R.P.H. Rettschnick. Determination of the barrier to intramolecular exciplex formation in a jet-cooled, bichromophoric molecule. *Chem. Phys. Lett.* **140**, 587, 1987.

Wegewijs, B., R.M. Hermant, J.W. Verhoeven, M.P. De Haas, J.M. Warman. Exciplex-type emission from folded and extended conformations of a donor-acceptor molecule with limited flexibility. *Chem. Phys. Lett.* **168**, 185, 1990.